



RESEARCH LETTER

10.1002/2015GL064503

Key Points:

- Airborne lidar measured phytoplankton layers in the marginal ice zone
- Layers were more prevalent and intense in open water than under pack ice
- There were abrupt transitions from surface bloom to subsurface layer

Correspondence to:

J. H. Churnside,
james.h.churnside@noaa.gov

Citation:

Churnside, J. H., and R. D. Marchbanks (2015), Subsurface plankton layers in the Arctic Ocean, *Geophys. Res. Lett.*, *42*, 4896–4902, doi:10.1002/2015GL064503.

Received 8 MAY 2015

Accepted 25 MAY 2015

Accepted article online 27 MAY 2015

Published online 22 JUN 2015

Subsurface plankton layers in the Arctic Ocean

James H. Churnside¹ and Richard D. Marchbanks²¹Earth System Research Laboratory, National Oceanographic and Atmospheric Administration, Boulder, Colorado, USA,²Cooperative Institute for Research in the Environmental Sciences, NOAA and University of Colorado Boulder, Boulder, Colorado, USA

Abstract The first synoptic measurements of subsurface plankton layers were made in the western Arctic Ocean in July 2014 using airborne lidar. Layers were detected in open water and in pack ice where up to 90% of the surface was covered by ice. Layers under the ice were less prevalent, weaker, and shallower than those in open water. Layers were more prevalent in the Chukchi Sea than in the Beaufort Sea. Three quarters of the layers observed were thinner than 5 m. The presence of these layers, which are not adequately captured in satellite data, will influence primary productivity, secondary productivity, fisheries recruitment, and carbon export to the benthos.

1. Introduction

The rate of warming in the Arctic is amplified by a number of feedback mechanisms [Pithan and Mauritsen, 2014; Serreze and Barry, 2011; Taylor et al., 2013]. As temperatures have warmed, sea ice has been shrinking in extent, getting thinner, and drifting more rapidly [Comiso, 2011; Kwok and Rothrock, 2009; Spreen et al., 2011; Vaughan et al., 2013]. The productivity of the Arctic Ocean, inferred from satellite observations, is increasing as a result of increases in ice-free area and phytoplankton growing season [Arrigo et al., 2008] and of thinning ice with more melt ponds [Arrigo et al., 2014]. Changes in subsurface plankton layers, not captured by satellite instruments, are not as clear. A better understanding of the prevalence, depths, and strengths of these layers is necessary to predict future CO₂ sequestration in the Arctic Ocean.

The existence of subsurface chlorophyll *a* maxima in the Arctic is well documented [Ardyna et al., 2013; Brown et al., 2015]. In the postbloom period of summer and early fall, nutrients are depleted at the surface and a subsurface layer develops at the thermocline [Brown et al., 2015; Hill and Cota, 2005; Martin et al., 2010]. In the Chukchi Sea, the surface bloom begins about 1 month before the sea ice retreats and is at a mean depth of 15 m by the time it does retreat, followed by a deepening of about 0.4 m d⁻¹ [Brown et al., 2015]. There is, of course, a lot of variability around this simplified picture.

While typical subsurface chlorophyll maximum are tens of meters thick [Cullen, 1982], there are also thin plankton layers that range in thickness from tens of centimeters to a few meters [Dekshenieks et al., 2001; Durham and Stocker, 2011; McManus et al., 2003]. Several mechanisms for formation have been described, including vertical current shear, water mass intrusions, buoyancy trapping, active swimming, and high localized growth rates. While most often observed in coastal waters, these layers also occur in the open ocean [Churnside and Donaghay, 2009; Durham and Stocker, 2011]. The concentration of chlorophyll in a thin layer can be as high as 55 times the background concentration [Ryan et al., 2008]. With this level of chlorophyll concentration, thin layers can have a large effect on local primary productivity, secondary productivity, fisheries recruitment, and carbon export to the benthos.

This paper describes observations of subsurface plankton layers in the western Arctic Ocean in July of 2014 using airborne lidar. The goals were to determine whether or not thin layers were present in the Arctic summer and to investigate the effects of sea ice on the thickness, depth, and strength of layers.

2. Methods

Subsurface plankton layers were detected with the same airborne lidar that has been used in previous investigations of subsurface plankton layers [Churnside and Ostrovsky, 2005; Churnside and Donaghay, 2009; Churnside et al., 2012]. This system produces profiles of copolarized and cross-polarized laser backscatter along the flight track with a depth resolution of approximately 1 m. For this investigation, the

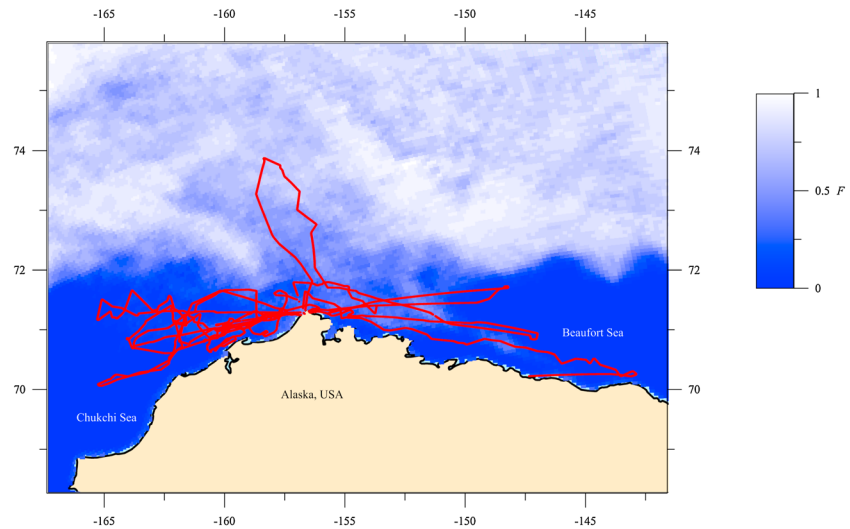


Figure 1. Lidar flight tracks (red lines) on map showing the average ice fraction from daily satellite images [Spren et al., 2008] for the last half of July 2014.

system was mounted in a NOAA Twin Otter and deployed to Barrow, Alaska, the last 2 weeks of July 2014. Flight altitude was 300 m and speed was 60 m s^{-1} . At the pulse-repetition frequency of 30 Hz, this speed provided profiles with a horizontal spacing of about 2 m. The total distance surveyed was over 4600 km.

Rather than follow a predetermined set of transects, each flight was adapted to current weather and ice conditions. The resulting areal coverage (Figure 1) shows that most flights were made toward open water to the west (five flights) or the east (three flights) out of Barrow, with one into the pack ice to the north. While there was a great deal of variability in the ice cover, the average of the daily satellite images over the last half of July in Figure 1 shows that open water was generally closer to Barrow in the Chukchi Sea than in the Beaufort Sea.

Layers were initially identified by visual inspection of the cross-polarized return, and each pulse within a layer was processed to obtain the layer characteristics. First, a linear regression of the logarithm of the measured photocathode current, $I_m(z)$, was used to estimate the background signal as

$$I_B(z) = I_B(0)\exp(-2\alpha z), \tag{1}$$

where z is the depth and α is the lidar attenuation coefficient. The depth range for the regression was from the surface to the depth at which $I_m(z)$ was 60 dB below the surface value. The bias introduced by including the effects of the layer in the regression is reduced by the logarithmic signal compression and will be neglected. The signal from the layer was obtained by subtracting the regression and correcting for the background attenuation:

$$I_L(z) = [I_m(z) - I_B(z)]\exp(2\alpha z). \tag{2}$$

The depth, D , and thickness, T , of the layer were obtained from the depth of the maximum value of $I_L(z)$ and its full width at half maximum, respectively. The thickness was then corrected for the effects of the 12 ns laser pulse length by deconvolution. Background subtraction was not applied to get the relative strength of the layer, which was defined as

$$S = \frac{I_m(D)}{I_B(D)}. \tag{3}$$

Note that S is also the ratio of the volume backscatter in the layer to the background value, because the calibration factor and attenuation both cancel. Values of D , T , and S were averaged over 1 km segments along the flight track for further analysis.

A bio-optical model was used to infer chlorophyll concentrations from the lidar return. For the lidar geometry used, the attenuation coefficient is very nearly approximated by the diffuse-attenuation coefficient, K_D , at the

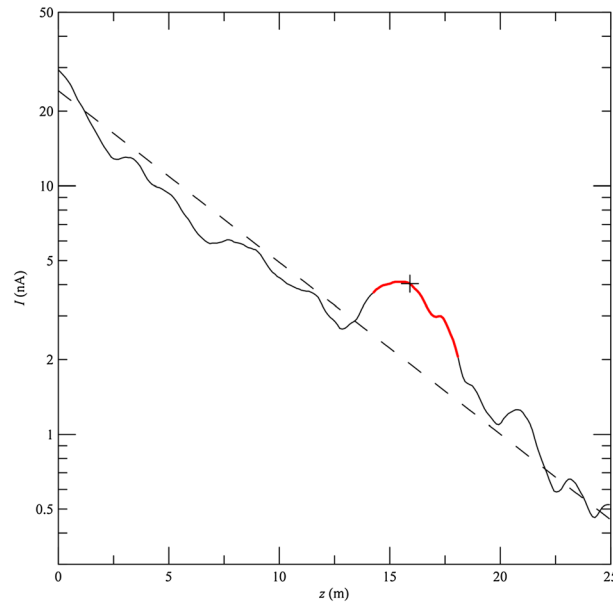


Figure 2. Example of lidar signal current, I_m (solid line), and background signal current, I_B (dashed line), as a function of depth z . The red segment is the extent of the layer as described in the text, and the plus sign marks the depth where the corrected layer signal, I_L , is greatest.

laser wavelength of 532 nm [Lee et al., 2013]. Thus, the background chlorophyll concentration can be estimated from Churnside et al. [2014] and Morel and Maritorena [2001]

$$C_B = \left(\frac{\alpha - 0.0452}{0.0474} \right)^{1.5}. \quad (4)$$

The corresponding volume scattering coefficient for the lidar geometry was estimated from Churnside et al. [2014] and Morel and Maritorena [2001]

$$\beta_B(\pi) = 1.94 \times 10^{-4} + [7 - 2.5 \log_{10}(C_B)] C_B^{0.766}. \quad (5)$$

The volume scattering coefficient for the layer was estimated by $\beta_L = S\beta_B$, and the total chlorophyll concentration in the layer, C_L , was estimated by inverting the relationship of equation (5). The chlorophyll enhancement in the layer was defined as the ratio C_L/C_B .

The processing steps are illustrated in the example of Figure 2. In this example, $I_m(z)$ was fit between $z=0$ and $z=28$ m to get $I_B(z)$. The layer extends from $z=14.3$ m to 18.1 m, with $D=15.9$ m and $T=3.6$ m after deconvolution. The attenuation of the fit is $\alpha=0.080 \text{ m}^{-1}$, so $C_B=0.62 \text{ mg m}^{-3}$ from equation (4). From equation (5), we obtained $\beta_B(\pi)=5.2 \times 10^{-4} \text{ m}^{-1} \text{ sr}^{-1}$. Since $S=2.1$ for this example, $\beta_L(\pi)=1.1 \times 10^{-3} \text{ m}^{-1} \text{ sr}^{-1}$, and we used equation (5) to get $C_L=3.36 \text{ mg m}^{-3}$; the chlorophyll enhancement factor is 5.4.

While the model was developed for unpolarized light, we applied it to our cross-polarized lidar channel. Problems with the copolarized channel made those data unreliable for the early flights. The error in the chlorophyll enhancement should be small if the depolarization is nearly constant. Comparing the enhancement estimated for both channels from the last flight, we found the average enhancement from the cross-polarized return to be 0.87 times that from the copolarized channel, but the difference was not significant ($P=0.10$). This difference is also smaller than the uncertainties inherent in the model, especially at high latitudes [Matsuoka et al., 2007; Mitchell, 1992; Wang et al., 2005].

The fraction of the surface covered by ice was estimated using the large difference between the reflectivity of ice and that of water. We counted the fraction of lidar shots in each kilometer of flight track where the surface reflectivity was above a threshold. The result was not sensitive to the values of the threshold chosen; the return from ice generally saturated the receiver. For the analysis, we considered a fraction $<10\%$ to be open water.

The fraction of the surface covered by ice was also estimated from satellite radiometry. Specifically, ice fraction was estimated from the 89 GHz channels on the Advanced Microwave Scanning Radiometer (AMSR-2) using the Arctic Radiation and Turbulence Interaction Study Sea Ice algorithm [Spreen et al., 2008]. Daily maps with 25 km resolution were used in the analysis.

3. Results

The prevalence of subsurface layers was higher in open water than in the pack ice. Figure 3 shows the probability of detecting a layer somewhere within a 1 km segment of flight track. Where the ice coverage is less than 10%, the probability is over 0.5. Where the ice coverage is greater than 10%, the average probability is 0.06. From the figure, it appears that the probability of detecting a layer decreases with increasing coverage between 10% and 100%; a linear regression returns a slope of -0.15 .

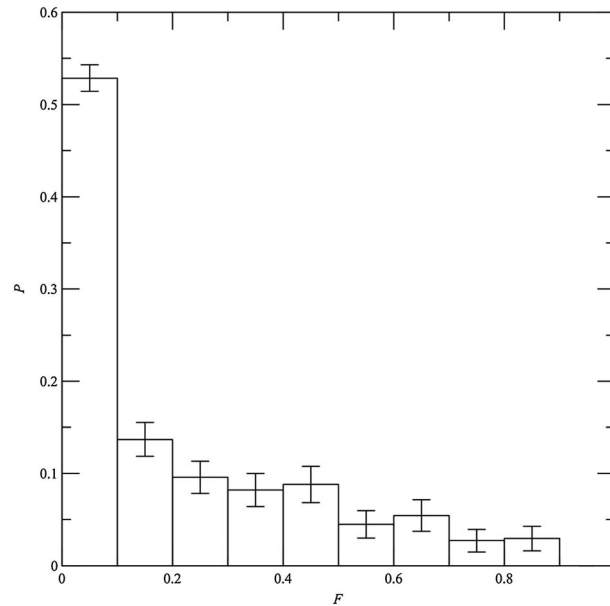


Figure 3. Probability of detecting a subsurface layer, P , as a function of the fraction of the surface covered by ice, F .

Layers were generally deeper in open water than under ice. For open water the mean depth (\pm sample standard deviation) was 19.6 ± 6.0 m. For the layers in ice the corresponding values were 15.6 ± 6.2 m. A Student's t test shows the difference of the means to be highly significant ($P < 10^{-18}$). The correlation between layer depth and ice fraction was not significant, however. We attribute this lack of correlation to the variability in ice fraction caused by changing winds. The spatial distribution of average layer depth (Figure 4) suggests that layers are deeper where persistent open water first appeared. This observation is reinforced by the correlation between layer depth and number of ice-free days between 1 July and the measurement of the layer. Taking only those layers with at least one ice-free day before the layer was detected, we obtained a correlation of 0.64 ($P < 10^{-32}$).

The chlorophyll enhancement was generally greater in open water than under ice. The distribution for both cases (Figure 5) shows a great deal of variability, but the difference between the mean values of 27.0 for open water and 8.9 for icy conditions is highly significant ($P < 10^{-32}$). Given the highly skewed distributions, the median values of 12.0 and 5.1 for the two cases may be a better indication of the differences.

The difference between the mean layer thickness in open water (3.8 m) and under ice (3.4 m) was statistically significant ($P = 0.004$), but probably does not have much practical importance. Of the layers detected, 34% would be considered thin according to the 3 m criteria we used previously [Churnside and Donaghay, 2009]. A higher fraction, 76%, would be considered thin using a limit of 5 m as suggested by Durham and Stocker [2011]. Recent work suggests that 5 m is a critical scale for phytoplankton layers, at least in coastal waters [Benoit-Bird et al., 2013].

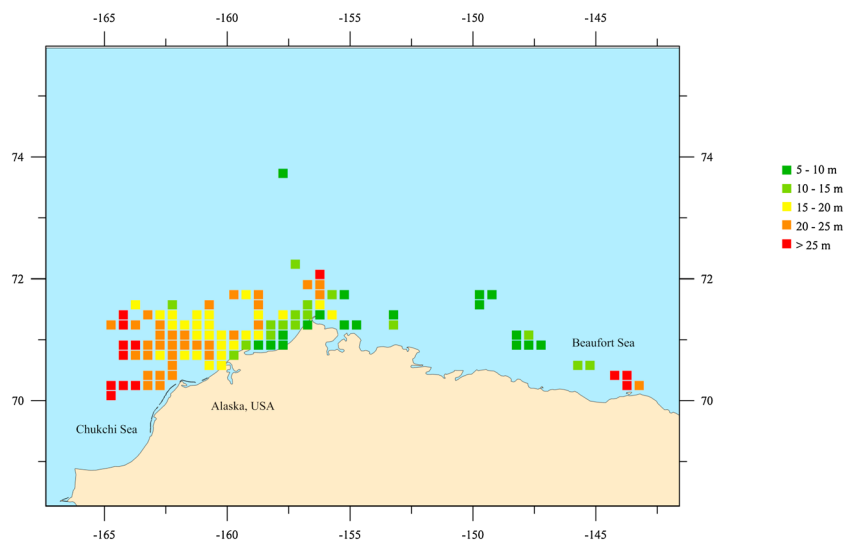


Figure 4. Map of layer depth averaged into 18.5 km square regions.

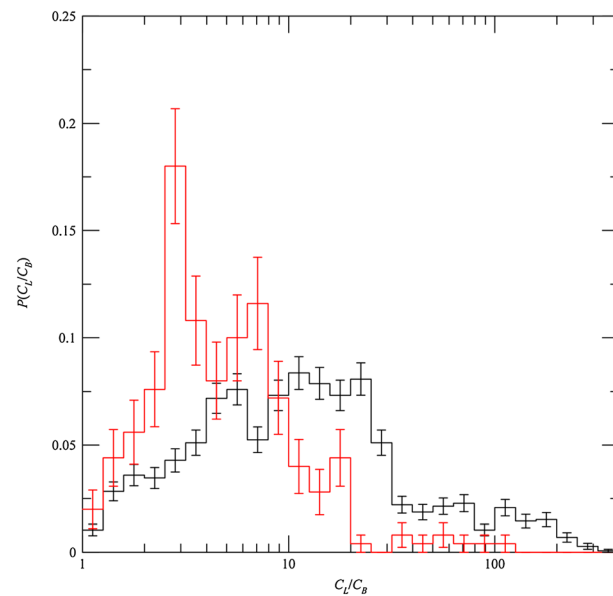


Figure 5. Probability distribution, P , of the chlorophyll enhancement, C_L/C_B for open water (black), and in the pack ice (red). Error bars were estimated from sampling error.

4. Discussion

When interpreting these data, the advantages and limitations of airborne lidar should be considered. The main advantage for our purposes is that the layer and ice properties are measured at the same place at the same time. This is particularly important when the pack ice is changing rapidly as winds shift. To illustrate, we note that the root-mean-square difference between lidar estimates of ice fraction and the nearest daily satellite estimates was 0.23. However, we have shown that the layer characteristics depend on the history of ice cover, and this can only be obtained from airborne lidar by repeated flights over the same area. The main limitation is the limited depth penetration of the lidar. This was generally between 20 and 40 m, with a maximum of 48 m. The overall average was 27 m (30 m for the Chukchi Sea).

While 48% of our survey effort was on the shelf waters of the Chukchi Sea, 87% of our observed layer segments were in this area, and it is reasonable to compare our results with previous observations in the Chukchi Sea [Brown *et al.*, 2015; Cota *et al.*, 1996; Coupel *et al.*, 2011; Hill and Cota, 2005]. Cota *et al.* [1996] noted that there was always a subsurface chlorophyll maximum (SCM) over the continental shelf in August and with ice fraction generally greater than 0.5. Hill and Cota reported a summertime depth of the SCM at about 25 m. Coupel *et al.* [2011] reported a SCM at all stations of the northern Chukchi shelf, with a typical depth of 15 m and a chlorophyll enhancement over surface waters of 2–10. Brown *et al.* [2015] reported SCM depths ranging from 3–106 m deep, with an average of 30 m but a mode of 15–20 m for the July data. These data suggest that the lidar may be missing some of the deeper SCMs, although these would not contribute significantly to overall primary productivity because of the low light levels.

The thickness of SCM layers is not often reported. Ardyna *et al.* [2013] presented expressions for averaged chlorophyll profiles that included Gaussian subsurface layers. The thickness of the average profile is much larger than the average of individual profile thickness, however, because of the variability of SCM depth. For the shallow-water cases, the expression is a numerical fit that should not be interpreted as a sum of contributions from a background concentration and a superimposed layer; the inferred background concentration would be negative in places. Martin *et al.* [2010] reported layer thickness in the Canadian Arctic with a range of 2–74 m and a median of 18 m. Brown *et al.* [2015] plotted an example of a profile on the Chukchi shelf with a peak chlorophyll concentration at 20 m depth, near the bottom of the pycnocline and a second, smaller peak at about 24 m. While not fully resolved, the upper peak has a width of 3.9 m, and both depth and thickness are consistent with our average values.

One spatial feature observed on a number of occasions was an abrupt transition between a strong surface layer and a subsurface layer, as in Figure 6. Within just a few hundred meters, a strong surface layer becomes a strong subsurface layer at a depth of about 12 m. This layer extends nearly continuously for almost 30 km along the flight track from open water on the left into the pack ice on the right. These abrupt transitions suggest an important role for horizontal mixing in the development of subsurface plankton layers.

A comparison of our data with previous observations suggests that there might be two types of subsurface chlorophyll layers in the Arctic postbloom period. The first is a thin layer associated with the pycnocline and affected by the physical processes described in the introduction. The second is a deep chlorophyll maximum that is associated with the nutricline later in the summer when the nutricline can become deeper than the

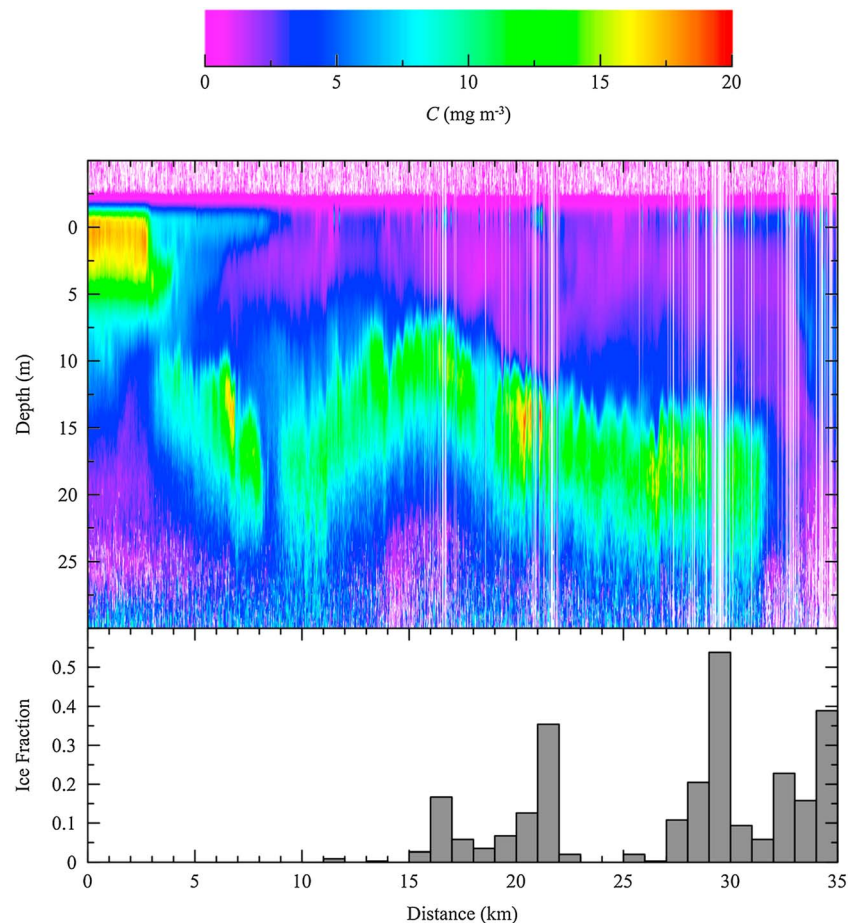


Figure 6. Chlorophyll concentration, C , as a function of depth and position along the flight track according to the color bar at the top. The vertical white lines denote missing data because of ice on the surface. The bar chart at the bottom provides the corresponding 1 km averaged fraction of the surface covered by ice.

pycnocline. The former is more detectable by airborne lidar. While these may exist simultaneously, only one would be identified with a subsurface chlorophyll maximum. Because of the higher light levels, the shallower layer may contribute more to column-integrated primary productivity. Thus, it seems likely that a combination of active and passive remote sensors could improve accuracy of primary productivity estimates in the Arctic Ocean as suggested by *Hill and Zimmerman* [2010].

Acknowledgments

Lidar data are available from the NOAA Earth System Research Laboratory archive (<http://www.esrl.noaa.gov/csd/groups/csd3/measurements/2014ArcticStratification>). AMSR-2 ice fraction data are available from the Institute of Environmental Physics at the University of Bremen (http://www.iup.uni-bremen.de:8084/ssmis/#Data_Archive). We would like to thank our NOAA pilots, Lt. Francisco Fuenmayor and En. Jacob Blaauboer, and mechanic, Sean Campbell.

The Editor thanks two anonymous reviewers for their assistance in evaluating this paper.

References

- Ardyna, M., M. Babin, M. Gosselin, E. Devred, S. Bélanger, A. Matsuoka, and J. É. Tremblay (2013), Parameterization of vertical chlorophyll a in the Arctic Ocean: Impact of the subsurface chlorophyll maximum on regional, seasonal, and annual primary production estimates, *Biogeosciences*, *10*(6), 4383–4404, doi:10.5194/bg-10-4383-2013.
- Arrigo, K. R., G. van Dijken, and S. Pabi (2008), Impact of a shrinking Arctic ice cover on marine primary production, *Geophys. Res. Lett.*, *35*, L19603, doi:10.1029/2008GL035028.
- Arrigo, K. R., et al. (2014), Phytoplankton blooms beneath the sea ice in the Chukchi sea, *Deep Sea Res., Part II*, *105*, 1–16, doi:10.1016/j.dsr2.2014.03.018.
- Benoit-Bird, K. J., E. L. Shroyer, and M. A. McManus (2013), A critical scale in plankton aggregations across coastal ecosystems, *Geophys. Res. Lett.*, *40*, 3968–3974, doi:10.1002/grl.50747.
- Brown, Z. W., K. E. Lowry, M. A. Palmer, G. L. van Dijken, M. M. Mills, R. S. Pickart, and K. R. Arrigo (2015), Characterizing the subsurface chlorophyll a maximum in the Chukchi Sea and Canada Basin, *Deep Sea Res., Part II*, doi:10.1016/j.dsr2.2015.02.010.
- Churnside, J. H., and P. L. Donaghay (2009), Thin scattering layers observed by airborne lidar, *ICES J. Mar. Sci.*, *66*(4), 778–789, doi:10.1093/icesjms/fsp029.
- Churnside, J. H., and L. A. Ostrovsky (2005), Lidar observation of a strongly nonlinear internal wave train in the Gulf of Alaska, *Int. J. Remote Sens.*, *26*(1), 167–177, doi:10.1080/01431160410001735076.
- Churnside, J. H., R. D. Marchbanks, J. H. Lee, J. A. Shaw, A. Weidemann, and P. L. Donaghay (2012), Airborne lidar detection and characterization of internal waves in a shallow fjord, *J. Appl. Remote Sens.*, *6*(1), 063611–063615, doi:10.1117/1.jrs.6.063611.

- Churnside, J. H., J. M. Sullivan, and M. S. Twardowski (2014), Lidar extinction-to-backscatter ratio of the ocean, *Opt. Express*, 22(15), 18,698–18,706, doi:10.1364/oe.22.018698.
- Comiso, J. C. (2011), Large decadal decline of the Arctic multiyear ice cover, *J. Clim.*, 25(4), 1176–1193, doi:10.1175/jcli-d-11-00113.1.
- Cota, G., L. Pomeroy, W. Harrison, E. Jones, F. Peters, W. J. Sheldon, and T. Weingartner (1996), Nutrients, primary production and microbial heterotrophy in the southeastern Chukchi Sea: Arctic summer nutrient depletion and heterotrophy, *Mar. Ecol. Prog. Ser.*, 135, 247–258, doi:10.3354/meps135247.
- Coupel, P., H. Y. Jin, D. Ruiz-Pino, J. F. Chen, S. H. Lee, H. L. Li, M. Rafizadeh, V. Garçon, and J. C. Gascard (2011), Phytoplankton distribution in the Western Arctic Ocean during a summer of exceptional ice retreat, *Biogeosci. Discuss.*, 8(4), 6919–6970, doi:10.5194/bgd-8-6919-2011.
- Cullen, J. L. (1982), The deep chlorophyll maximum: Comparing vertical profiles of chlorophyll a, *Can. J. Fish. Aquat. Sci.*, 39, 791–803.
- Deksheniaks, M. M., P. L. Donaghay, J. M. Sullivan, J. E. B. Rines, T. R. Osborn, and M. S. Twardowski (2001), Temporal and spatial occurrence of thin phytoplankton layers in relation to physical processes, *Mar. Ecol. Prog. Ser.*, 223, 61–71, doi:10.3354/meps223061.
- Durham, W. M., and R. Stocker (2011), Thin phytoplankton layers: Characteristics, mechanisms, and consequences, *Annu. Rev. Mar. Sci.*, 4(1), 177–207, doi:10.1146/annurev-marine-120710-100957.
- Hill, V., and G. Cota (2005), Spatial patterns of primary production on the shelf, slope and basin of the Western Arctic in 2002, *Deep Sea Res., Part II*, 52(24–26), 3344–3354, doi:10.1016/j.dsr2.2005.10.001.
- Hill, V. J., and R. C. Zimmerman (2010), Estimates of primary production by remote sensing in the Arctic Ocean: Assessment of accuracy with passive and active sensors, *Deep Sea Res., Part I*, 57(10), 1243–1254, doi:10.1016/j.dsr.2010.06.011.
- Kwok, R., and D. A. Rothrock (2009), Decline in Arctic sea ice thickness from submarine and ICESat records: 1958–2008, *Geophys. Res. Lett.*, 36, L15501, doi:10.1029/2009GL039035.
- Lee, J. H., J. H. Churnside, R. D. Marchbanks, P. L. Donaghay, and J. M. Sullivan (2013), Oceanographic lidar profiles compared with estimates from in situ optical measurements, *Appl. Opt.*, 52(4), 786–794, doi:10.1364/AO.52.000786.
- Martin, J., J. Tremblay, J. Gagnon, G. Tremblay, A. Lapoussi, C. Jose, M. Poulin, M. Gosselin, Y. Gratton, and C. Michel (2010), Prevalence, structure and properties of subsurface chlorophyll maxima in Canadian Arctic waters, *Mar. Ecol. Prog. Ser.*, 412, 69–84, doi:10.3354/meps08666.
- Matsuoka, A., Y. Huot, K. Shimada, S.-I. Saitoh, and M. Babin (2007), Bio-optical characteristics of the western Arctic Ocean: Implications for ocean color algorithms, *Can. J. Remote Sens.*, 33(6), 503–518, doi:10.5589/m07-059.
- McManus, M. A., et al. (2003), Characteristics, distribution and persistence of thin layers over a 48 hour period, *Mar. Ecol. Prog. Ser.*, 261, 1–19, doi:10.3354/meps261001.
- Mitchell, B. G. (1992), Predictive bio-optical relationships for polar oceans and marginal ice zones, *J. Mar. Syst.*, 3(1–2), 91–105, doi:10.1016/0924-7963(92)90032-4.
- Morel, A., and S. Maritorena (2001), Bio-optical properties of oceanic waters: A reappraisal, *J. Geophys. Res.*, 106(C4), 7163–7180, doi:10.1029/2000JC000319.
- Pithan, F., and T. Mauritsen (2014), Arctic amplification dominated by temperature feedbacks in contemporary climate models, *Nat. Geosci.*, 7(3), 181–184, doi:10.1038/ngeo2071.
- Ryan, J. P., M. A. McManus, J. D. Paduan, and F. P. Chaves (2008), Phytoplankton thin layers caused by shear infrontal zones of a coastal upwelling system, *Mar. Ecol. Prog. Ser.*, 354, 21–34, doi:10.3354/meps0722.
- Serreze, M. C., and R. G. Barry (2011), Processes and impacts of Arctic amplification: A research synthesis, *Global Planet. Change*, 77(1–2), 85–96, doi:10.1016/j.gloplacha.2011.03.004.
- Spreen, G., L. Kaleschke, and G. Heygster (2008), Sea ice remote sensing using AMSR-E 89-GHz channels, *J. Geophys. Res.*, 113, C02S03, doi:10.1029/2005JC003384.
- Spreen, G., R. Kwok, and D. Menemenlis (2011), Trends in Arctic sea ice drift and role of wind forcing: 1992–2009, *Geophys. Res. Lett.*, 38, L19501, doi:10.1029/2011GL048970.
- Taylor, P. C., M. Cai, A. Hu, J. Meehl, W. Washington, and G. J. Zhang (2013), A decomposition of feedback contributions to polar warming amplification, *J. Clim.*, 26(18), 7023–7043, doi:10.1175/jcli-d-12-00696.1.
- Vaughan, D. G., et al. (2013), Observations: Cryosphere, in *Climate Change 2013: The Physical Science Basis. Contribution of Working Group I to the Fifth Assessment Report of the Intergovernmental Panel on Climate Change*, edited by T. F. Stocker et al., pp. 317–382, Cambridge Univ. Press, Cambridge.
- Wang, J., G. F. Cota, and D. A. Ruble (2005), Absorption and backscattering in the Beaufort and Chukchi Seas, *J. Geophys. Res.*, 110, C04014, doi:10.1029/2002JC001653.